Blind Image Deblurring with Outlier Handling Supplemental Material

Jiangxin Dong[1] Jinshan Pan[2] Zhixun Su[1,4] Ming-Hsuan Yang[3]
[1]Dalian University of Technology [2]Nanjing University of Science and Technology [3]UC Merced
[4]Guilin University of Electronic Technology
dongjxjx@gmail.com sdluran@gmail.com zxsu@dlut.edu.cn mhyang@ucmerced.edu

Overview

In this supplemental material, we analyze how the proposed blind image deblurring method performs on images with outliers and demonstrate the effectiveness of the proposed data fidelity term in Section 1. Section 2 provides more analysis of the proposed algorithm. We quantitatively evaluate the proposed algorithm and compare it against existing blind deblurring methods on the datasets with outliers and random noise in Section 3. We further evaluate the proposed method on publicly available datasets [8] as well as [15] and show that it performs well against the state-of-the-art deblurring methods in Section 4. The proposed non-uniform deblurring algorithm is presented in Sections 5. More visual comparisons are shown in Section 6.

1. Effectiveness of Proposed Method

As discussed in Section 4 of the main paper, existing outlier handling methods [2, 16] address the effects of outliers in non-blind deblurring and their straightforward extensions do not perform well for blind image deblurring (see Figure 1, *i.e.*, Figure 8 in the main paper). To process blurred images with outliers in blind image deblurring, most state-of-the-art methods depend on extra steps of light streak detection [6, 10], salient edge selection [12], and outlier detection [12]. As discussed in the main paper, the main idea of the state-of-the-art method [12] is the edge selection and outlier detection. These two ad-hoc operations are not derived from the original optimization problem and increase the complexity of kernel estimation. [12] is less effective when useful edges are not extracted (Figure 2(b), (d)-(f)). This limitation has also been discussed by [12] in the supplemental material. In addition, the deconvolution model with an ℓ_1 norm-based data term is the bottleneck as the images estimated by this model significantly affect the following edge selection and outlier detection steps. As the ℓ_1 norm-based data term is less robust to saturated pixels [2], the intermediate latent images by [12] usually contain significant artifacts (Figure 2(g)-(i)). This increases the difficulty for the ad-hoc edge-selection method [12] as it is difficult to find a good threshold to remove artifacts. Although the outlier detection step is able to detect those artifacts, it is likely that most edges are removed after applying outlier detection (Figure 2(f)). This usually occurs when blurred images contain saturated pixels as the ℓ_1 norm-based data fidelity term is less robust to saturated pixels.

In contrast, we propose a robust outlier handling method based on a robust data fidelity term, which can minimize the effects of outliers on the blur kernel estimation (see Figure 2(g)-(o)). Our method is motivated by the properties of outliers and its effect on data terms. It does not need ad-hoc selection steps and is derived from a unified optimization problem with a robust data term. As discussed in Section 4.1 of the main paper, from both the mathematical essence of the robust function $\mathcal{R}(\cdot)$ and the perspective of the IRLS optimization, the outliers have less effect on both the intermediate latent image estimation and the blur kernel estimation within the proposed framework. These properties ensure that the proposed deblurring algorithm based on the proposed dada fidelity term is able to handle outliers. The comparisons in Figure 2 show that our method can minimize the effect of outliers on kernel estimation and recover clearer structures with fewer artifacts.

(a) Blurred image (b) [1]+[2] (c) Extension of [2]

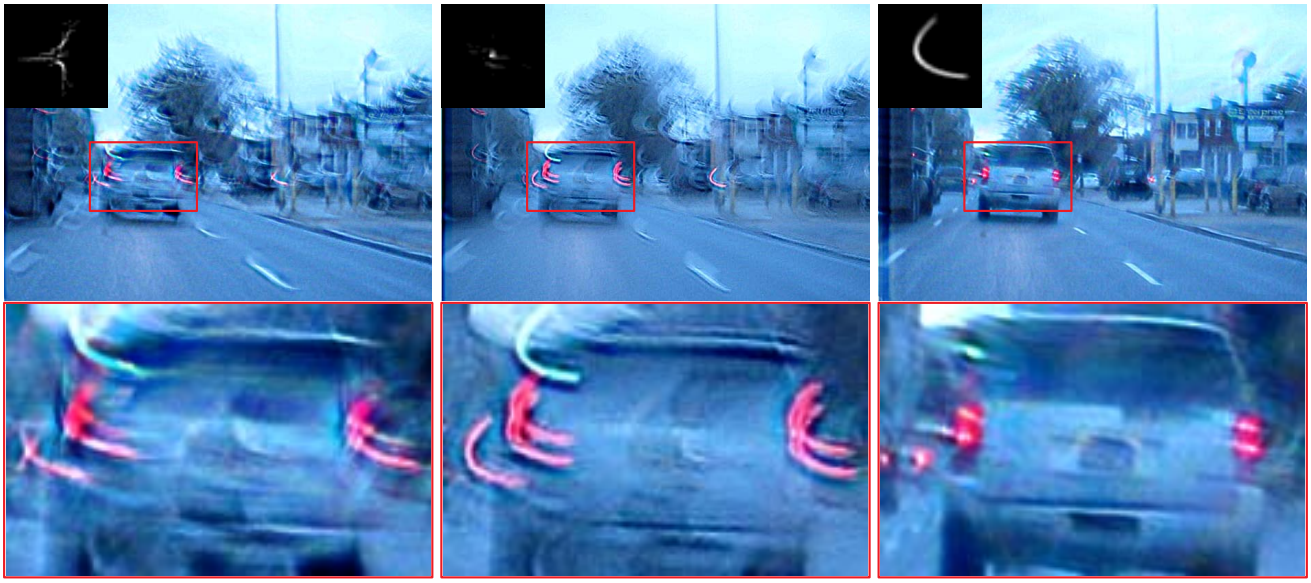

(d) [1]+[16] (e) Extension of [16] (f) Ours

Figure 1. Comparison with Cho *et al*. [2] and Whyte *et al*. [16] and their straightforward extensions. The results show that straightforward extensions of these methods do not generate clear images.

(a) Blurred image (b) Results of [12] (c) Ours

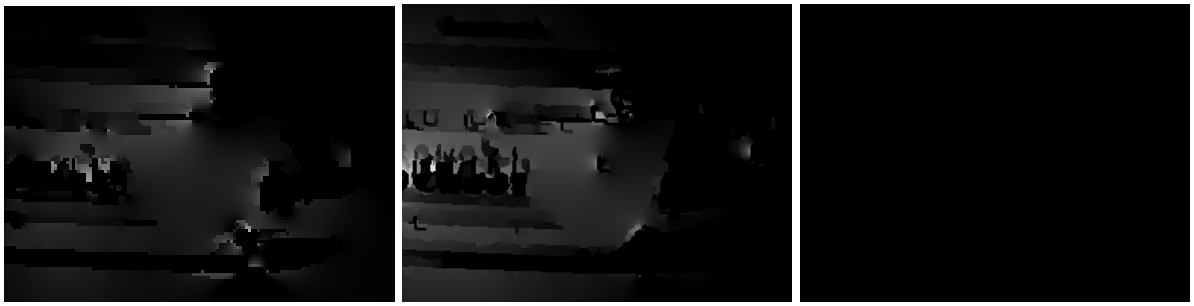

(d) (e) (f)

(g) (h) (i)

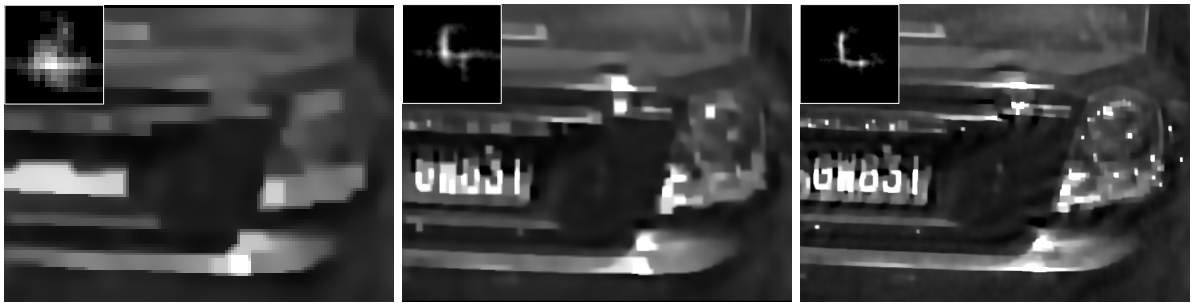

(j) (k) (l)

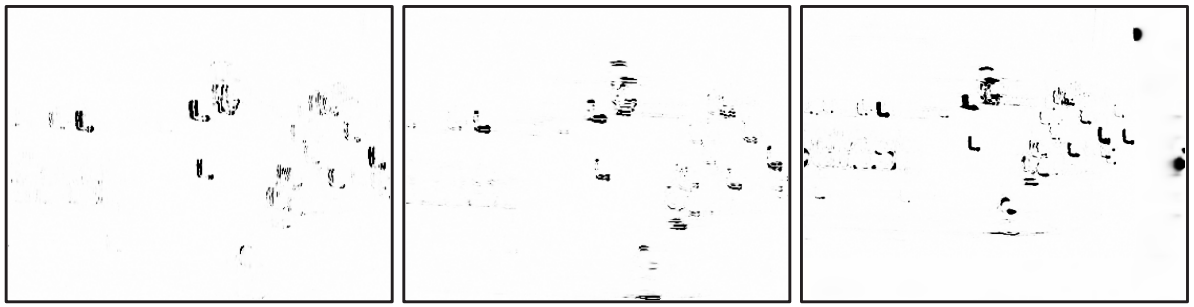

(m) ω_h^k (n) ω_v^k (o) ω^x

Figure 2. Comparison with Pan *et al*. [12]. (d)-(f) Edge selection results during the iterations by [12]. (g)-(i) and (j)-(l) Intermediate latent images with estimated kernels during the iterations by [12] and the proposed method, respectively. (m)-(o) Weight maps (see Section 3.1 and 3.2 in the main paper) of the proposed method in the kernel estimation and the latent image estimation. The proposed method generates a clear image with fine details and the weights derived from the IRLS iteration are able to handle outliers.

2. Further Analysis on the Proposed Method

In this section, we provide more analysis on the proposed method in terms of the running time (Section 2.1), the robust function used in the data fidelity term (Section 2.2), the effectiveness on the noise-free images (Section 2.3) and the limitations of the proposed method (Section 2.4).

2.1. Running Time

As deblurring images with significant outliers is very challenging, the run time of deblurring methods designed for this problem is not fast. We compare our method with the outlier handling methods in Table 1. Table 1 shows that our method compares favorably against competing methods, in addition to better-restored results.

Table 1. Running time (/s) and PSNR comparisons on the same PC. The size of the test image is of 800×800 pixels. The results show that our method compares favorably against competing outlier handling methods, in addition to better-restored results.

Method	Time	PSNR
Levin *et al*. [9] (Matlab)	244.55	23.77
Zhong *et al*. [19] (Matlab)	46.79	22.24
Pan *et al*. [13] (Matlab)	731.56	29.11
Pan *et al*. [12] (Matlab)	688.73	17.79
Ours (Matlab)	497.44	**31.21**

2.2. Further Analysis on the Proposed Data Fidelity Term

Note that although a truncated ℓ_2-norm has the similar shape to $\mathcal{R}(z)$, the truncated ℓ_2-norm based data fidelity term is different from the proposed data fidelity term. Our data fidelity term is continuously differentiable, and its weight in the IRLS method is able to detect the regions of outliers (see Section 4.1 in the manuscript and Figure 2). However, the truncated ℓ_2-norm based data fidelity term is not differentiable and does not have these properties. To further demonstrate the effectiveness of the proposed data fidelity term, we compare it with the truncated ℓ_2-norm based data fidelity term on the proposed dataset with impulse noise. Figure 3 shows that the blind image deblurring method using the truncated ℓ_2-norm based data fidelity term is less effective for blurred images with outliers. In contrast, the proposed algorithm generates results with higher PSNR values. Figure 4 shows visual comparisons. The deblurred results generated by the truncated ℓ_2-norm based data fidelity term

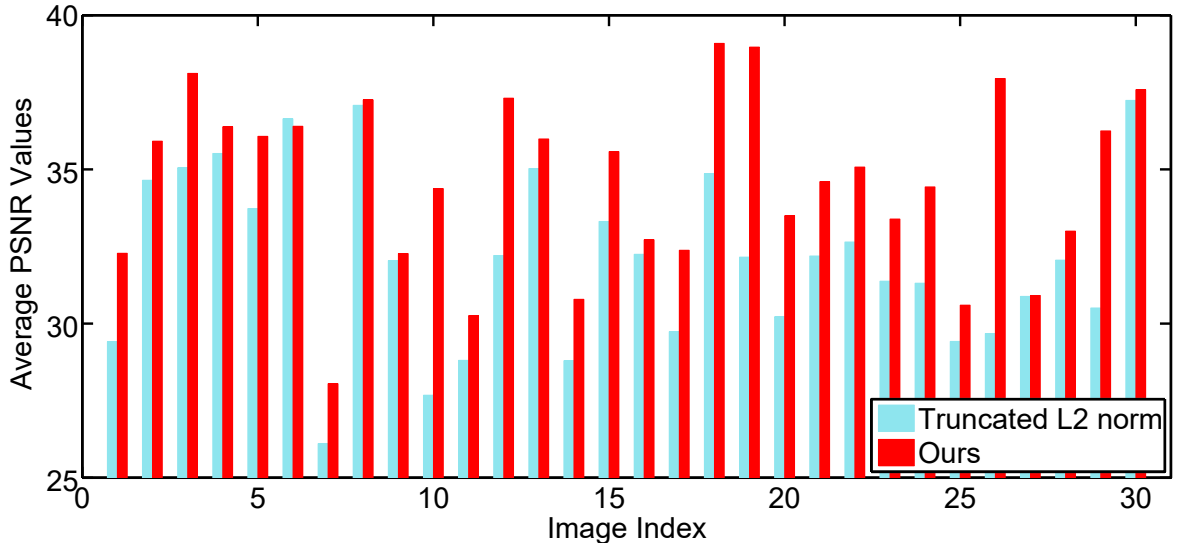

Figure 3. Quantitative evaluation of the proposed data fidelity term and the truncated ℓ_2-norm based data fidelity term on the proposed dataset with impulse noise. The proposed data fidelity term is continuously differentiable, and its weight in the IRLS method is able to detect the regions of outliers (see Section 4.1 in the manuscript and Figure 2). However, the truncated ℓ_2-norm based data fidelity term is not differentiable and does not have these properties. Thus, the results generated by this method have lower PSNR values.

(a) Blurred image (b) Truncated ℓ_2-norm (c) Ours (d) Blurred image (e) Truncated ℓ_2-norm (f) Ours

Figure 4. A visual comparison with the truncated ℓ_2-norm based data fidelity term. (b) and (e): Results by the truncated ℓ_2-norm based data fidelity term. (c) and (f): Our results.

contain significant ringing artifacts and blur residues. In contrast, the proposed algorithm generates clearer results with fine textures.

2.3. Effectiveness on Noise-Free Images

For blurred images without outliers, the intermediate latent images may contain artifacts due to inaccurate kernel estimation, especially in the first few iterations. The values of $x * k - y$ will be large at the positions of artifacts. Thus, the weights (w^x, w_h^k, w_v^k) in (7) and (9) are small. This indicates that the effect of artifacts is minimized in the following steps, thereby facilitating kernel estimation.

Figure 5 shows an example to demonstrate the effect of our method on an outlier-free image. Even for the noise-free image, the intermediate latent images in the first few iterations can contain artifacts (Figure 5(d) and (g)), which are one kind of outliers. However, the outlier detection method by [12] does not detect these artifacts (Figure 5(j)). In contrast, based on the proposed data fidelity term, the weights for these artifacts in our kernel estimation are small (Figure 5(h)-(i)). Therefore, as discussed in Section 4 of the main paper, the effect of artifacts is minimized in the following steps, thereby facilitating kernel estimation.

2.4. Limitations of the Proposed Method

The proposed method is likely to fail when the saturated area is too large. Figure 6 shows an example where the saturated areas are very large. The result generated by our method is almost the same as the blurred image, which indicates that our method is less effective for images with very large saturated areas.

3. Quantitative Evaluations on Datasets with Outliers

Dataset with saturated pixels. To evaluate the effectiveness of the proposed method, we create a dataset containing 5 ground truth low-light images (see Figure 7) with saturated pixels and 8 kernels from [8] (see Figure 8). Similar to [12], each ground truth image is synthetically blurred by 8 different blur kernels and high-intensity pixels are clipped. We also add 1% random noise on each blurred image. For fair comparisons, we use the original implementations of the state-of-the-art methods [1, 6, 11, 12, 13, 18] to estimate blur kernels. The non-blind deblurring method [2] is used to generate the final deblurring results. Figure 9 and Table 2 show that the proposed algorithm achieves favorable results compared with the state-of-the-art methods.

Dataset with impulse noise. To further evaluate the proposed method, we create a dataset containing 30 ground truth natural images (see Figure 10) and 8 kernels from [8], in which we add the impulse noise (as it is one of the most common non-Gaussian noise) to each image. The noise density is set to be 0.02. Thus, we have 240 blurred images in total. We evaluate the proposed algorithm against several state-of-the-art deblurring methods including the outlier handling method [12]. We follow the protocol used in the dataset with saturated pixels for fair comparisons. The PSNR and error ratio [8] are used as the quality metric. Figure 11, Table 3 and Figure 12 show that our method performs favorably against the state-of-the-art methods.

Robustness of the proposed algorithm. We further evaluate the proposed algorithm using images with different noise densities. Figure 13 shows that the proposed algorithm performs well even when the noise density is high.

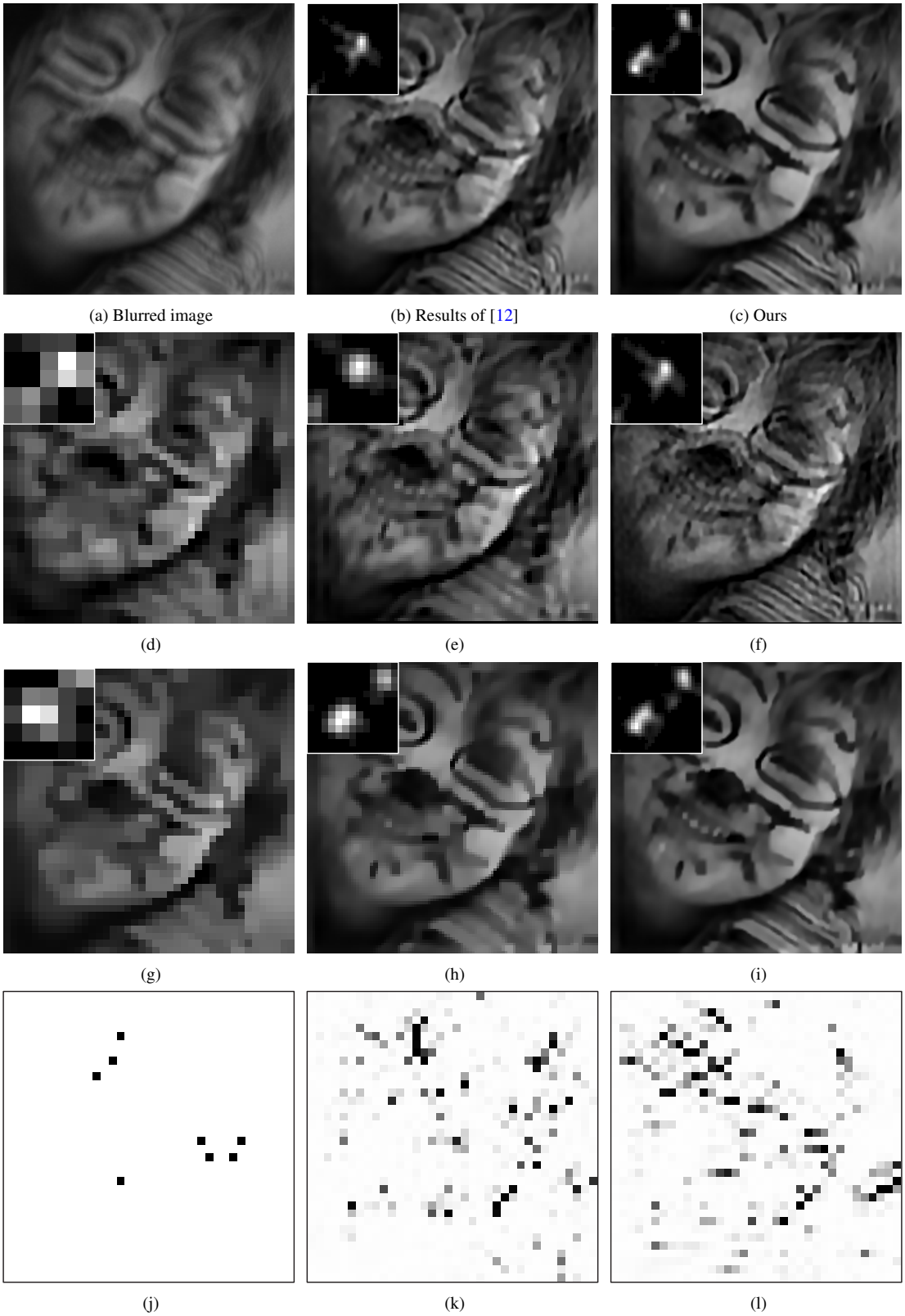

(a) Blurred image (b) Results of [12] (c) Ours

(d) (e) (f)

(g) (h) (i)

(j) (k) (l)

Figure 5. Effectiveness on a noise-free image. (d)-(f) and (g)-(i) Intermediate latent images with estimated kernels during the iterations by [12] and the proposed method, respectively. (j) Outlier detection mask by [12]. (k)-(l) Weight maps (see Section 3.2 in the main paper) of the proposed method in the kernel estimation. The proposed method generates a clear image with fine details and the weights derived from the IRLS iteration are able to handle outliers.

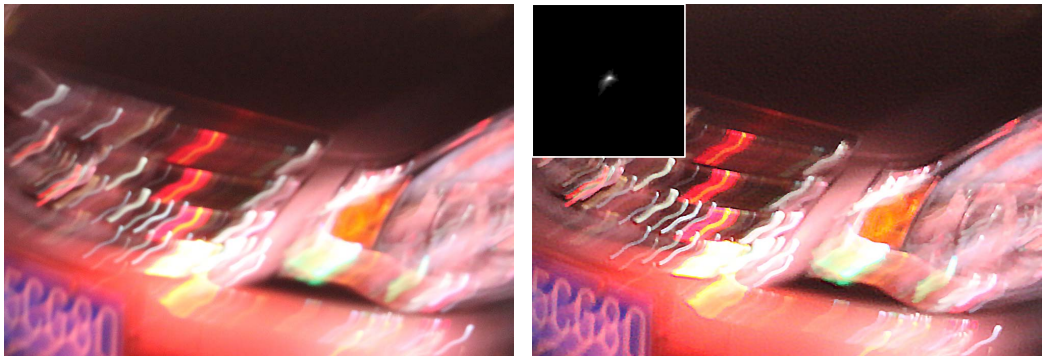

Figure 6. The limitation of our method. Our method is less effective when the saturated areas are very large.

Figure 7. Ground truth images that are used in the synthetic image dataset with saturated pixels.

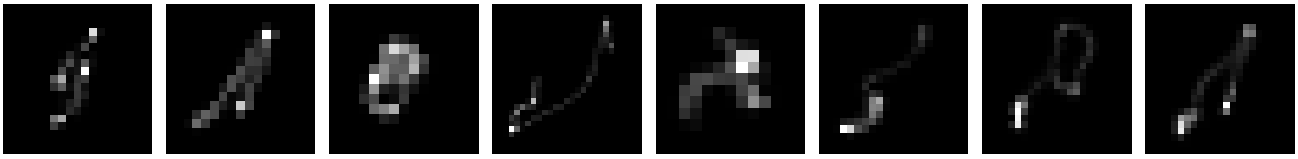

Figure 8. Ground truth kernels form [8].

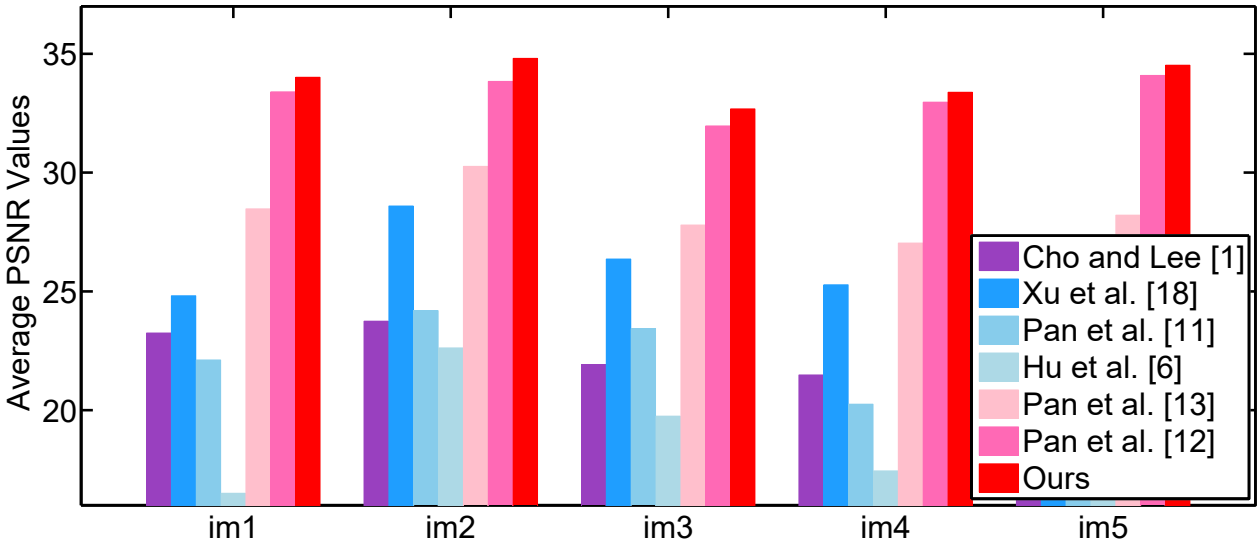

Figure 9. Quantitative evaluation on the dataset with saturated pixels in terms of PSNR. The proposed method generates the results with higher PSNR values.

Figure 10. Ground truth images that are used in the synthetic dataset impulse noise.

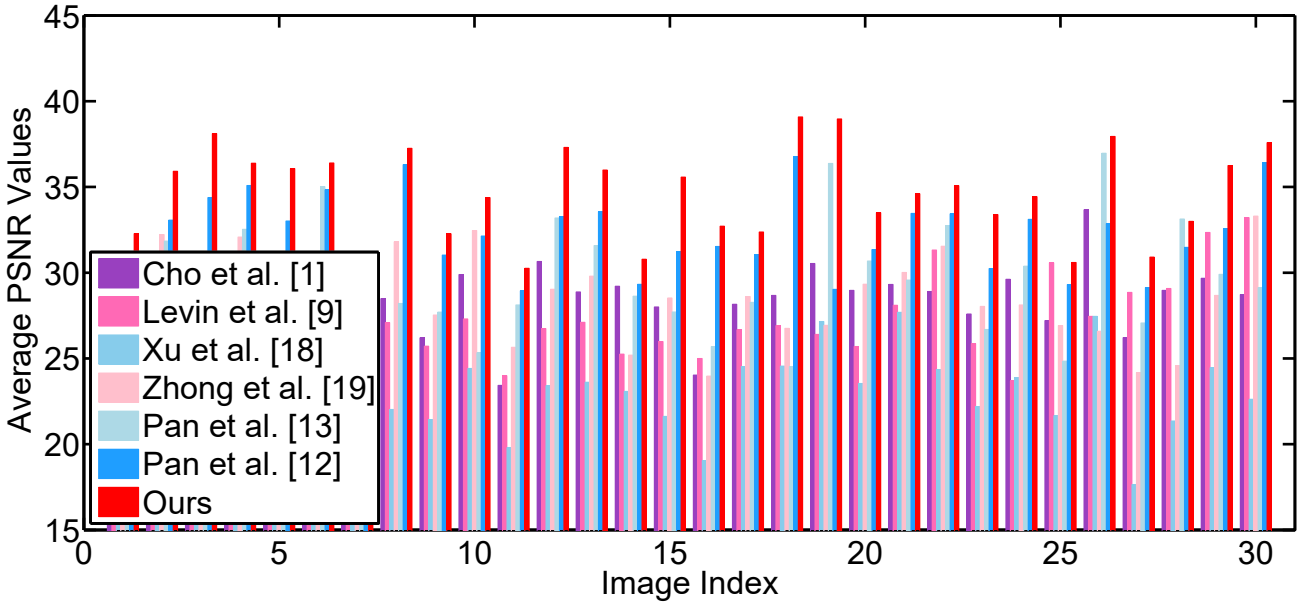

Figure 11. Quantitative evaluation on the dataset with impulse noise in terms of PSNR. The proposed method generates the results with higher PSNR values.

Table 2. Quantitative comparison using the dataset with saturated pixels in terms of error ratio metric.

	[1]	[18]	[11]	[6]	[13]	[12]	Ours
Average Error Ratio	18.04	7.42	13.41	34.37	3.83	3.22	**3.09**

Table 3. Quantitative comparison on the proposed dataset with impulse noise in terms of PSNR.

	[1]	[9]	[18]	[19]	[13]	[12]	Ours
Average PSNR	28.5819	27.1834	30.6736	28.5304	29.3544	32.0176	**34.5818**

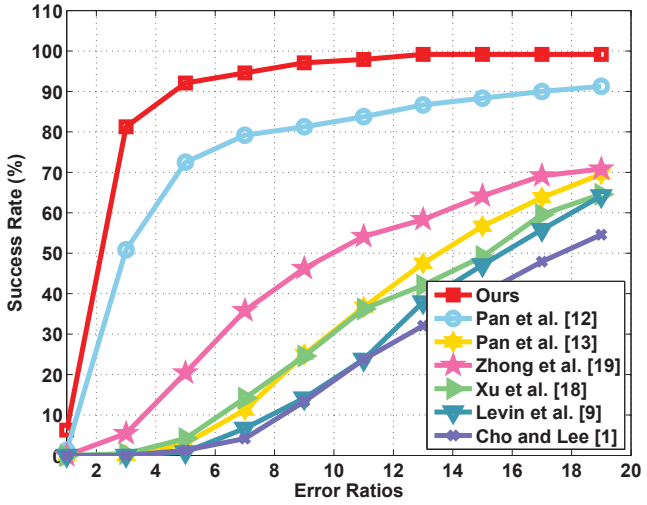

Figure 12. Quantitative evaluation on the dataset with impulse noise.

4. Quantitative Evaluation on the Natural Image Deblurring Datasets

We evaluate our method on the natural image deblurring datasets [8] and [15]. The natural image deblurring dataset [8] contains 4 ground truth images and 8 blur kernels. The natural image dataset [15] involves 640 blurred images. Figures 14 and 15 demonstrates that the proposed algorithm performs favorably against the state-of-the-art methods.

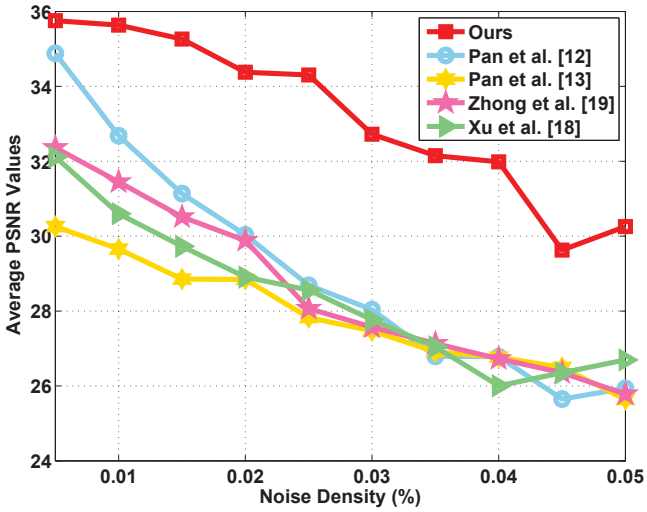

Figure 13. Robustness of the proposed algorithm.

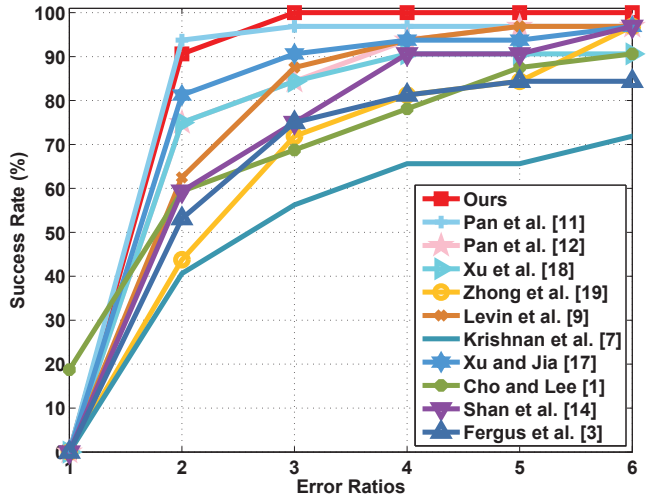

Figure 14. Quantitative evaluation on the benchmark dataset [9].

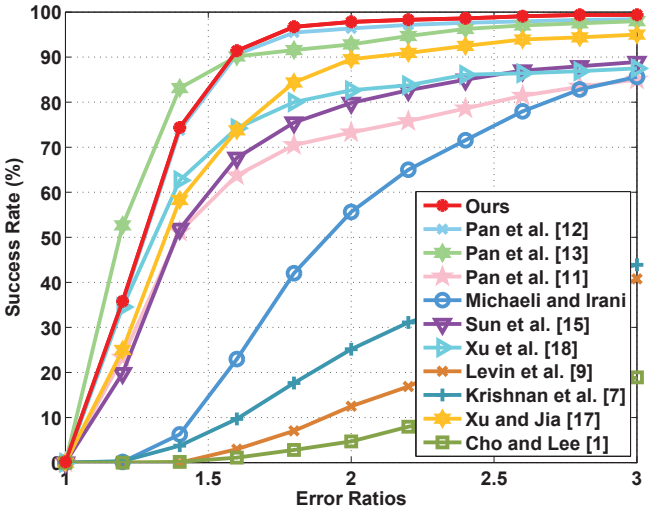

Figure 15. Quantitative evaluation on the benchmark dataset [15].

5. Non-Uniform Deblurring Algorithm

As mentioned in the main paper, our non-uniform deblurring process is carried out by alternatively solving

$$\min_{\mathbf{x}} \mathcal{R}(\mathbf{K}\mathbf{x} - \mathbf{y}) + \lambda \|\nabla \mathbf{x}\|_{0.8} \tag{1}$$

and

$$\min_{\mathbf{k}} \mathcal{R}(\mathbf{A}\mathbf{k} - \mathbf{y}) + \gamma \|\mathbf{k}\|_1. \tag{2}$$

Estimating latent image: For (1), we follow the solver of (6) in the main paper and use the IRLS method to solve (1). At each iteration, we need to solve the quadratic problem:

$$\mathbf{x}^{[t+1]} = \operatorname*{argmin}_{\mathbf{x}} \sum_{\mathrm{p}} \{\omega^{\mathbf{x}} |(\mathbf{K}\mathbf{x} - \mathbf{y})_{\mathrm{p}}|^2 + \lambda(\omega_h^{\mathbf{x}} |(\partial_h \mathbf{x})_{\mathrm{p}}|^2 + \omega_v^{\mathbf{x}} |(\partial_v \mathbf{x})_{\mathrm{p}}|^2)\}, \tag{3}$$

where $\omega^{\mathbf{x}} = \frac{\mathcal{R}'((\mathbf{K}\mathbf{x}^{[t]} - \mathbf{y})_{\mathrm{p}})}{(\mathbf{K}\mathbf{x}^{[t]} - \mathbf{y})_{\mathrm{p}}}$, $\mathcal{R}'(\cdot)$ is the derivative function of $\mathcal{R}(\cdot)$, $\omega_h^{\mathbf{x}} = |(\partial_h \mathbf{x}^{[t]})_{\mathrm{p}}|^{-1.2}$, $\omega_v^{\mathbf{x}} = |(\partial_v \mathbf{x}^{[t]})_{\mathrm{p}}|^{-1.2}$, t denotes the iteration index, and the subscript p denotes the spatial location of a pixel.

To efficiently solve the minimization (3), we first calculate the matrix $\mathbf{K}$. As is assumed by the method [5], the blur kernels at a small region are similar and can be approximated by the locally uniform blur mode. It divides the image into M patches and $\mathbf{K}$ can be represented by

$$\mathbf{K} = \sum_{m=1}^{M} \mathrm{diag}(\mathcal{W}_m)\mathbf{K}_m, \tag{4}$$

where $\mathrm{diag}(z)$ is a diagonal matrix with the element of vector z on the main diagonal, $\mathcal{W}_m$ is a window function and has the same size as $\mathbf{x}$, which satisfies $\sum_m \mathcal{W}_m = 1$, and $\mathbf{K}_m$ is the matrix corresponding to the blur kernel k_m for the m-th patch. To compute $\mathbf{K}$ using FFTs, $\mathbf{K}$ can be expressed as

$$\mathbf{K} = \mathbf{Z}_p^{\top} \sum_{m=1}^{M} \mathbf{C}_m^{\top}(\mathcal{F}^{-1}(\mathrm{diag}(\mathcal{F}(\mathbf{Z}_a k_m))))\mathcal{F}(\mathbf{C}_m \mathrm{diag}(\mathcal{W}_m)). \tag{5}$$

where $\mathbf{C}_m(\cdot)$ is a matrix that chops the m-th patch from a vector, $\mathbf{C}_m^{\top}(\cdot)$ is a matrix that paste the m-th patch to original vector, $\mathbf{Z}_p$ is the zero-padding matrix that prepends zeros to a vector such that its size matches the size of the vector resulting from the summation, and $\mathbf{Z}_a$ is a zero-padding matrix that appends zeros to a vector that its size matches the patch size.

By (5) of $\mathbf{K}$, the solution (3) can be solved by the conjugate gradient method. The algorithm for solving (1) is the same as Algorithm 1, where we only need to replace (7) with (3).

Estimating blur kernel: For the optimization of the kernel estimation model (2), we use the IRLS method to solve (2). At each iteration, we use same optimization proposed by [18] to estimate $\mathbf{k}$. The proposed non-uniform deblurring method is achieved by alternatively minimizing (1) and (2). We use the same settings as the uniform deblurring in Algorithm 1.

6. More Experimental Results

In this section, we show more deblurred results by the proposed algorithm and the state-of-the-art methods, in addition to the examples of the proposed datasets in Figures 7 and 10.

(a) Blurred image (b) Cho and Lee [1] (c) Krishnan *et al*. [7]

(d) Levin *et al*. [9] (e) Xu *et al*. [18] (f) Zhong *et al*. [19]

(g) Goldstein and Fattal [4] (h) Pan *et al*. [11] (i) Hu *et al*. [6]

(j) Pan *et al*. [13] (k) Pan *et al*. [12] (l) Ours

Figure 16. Deblurred results on one synthetic image with numerous saturated areas and random noise. The proposed method generates clear images with fewer ringing artifacts.

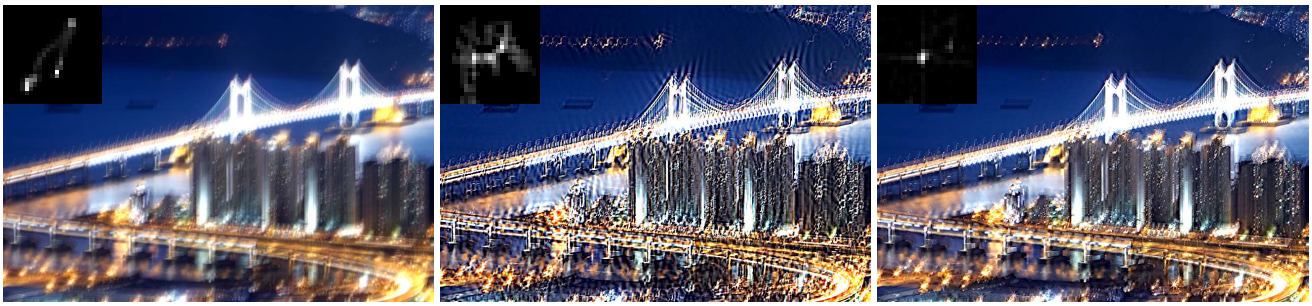

(a) Blurred image (b) Cho and Lee [1] (c) Krishnan *et al*. [7]

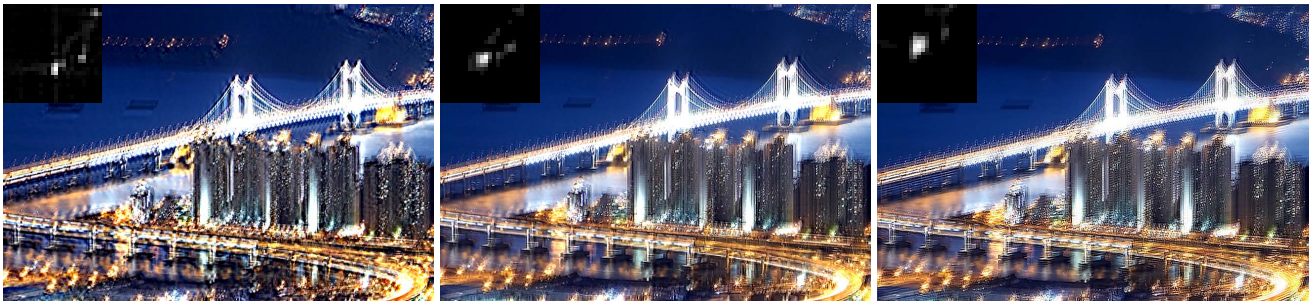

(d) Levin *et al*. [9] (e) Xu *et al*. [18] (f) Zhong *et al*. [19]

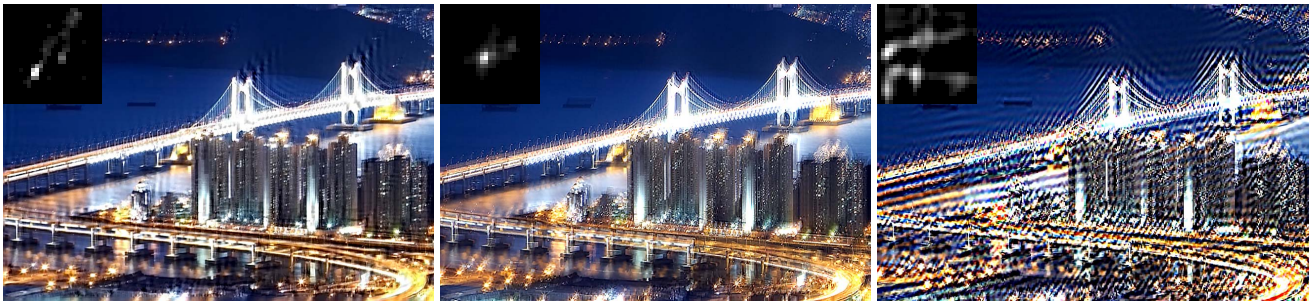

(g) Goldstein and Fattal [4] (h) Pan *et al*. [11] (i) Hu *et al*. [6]

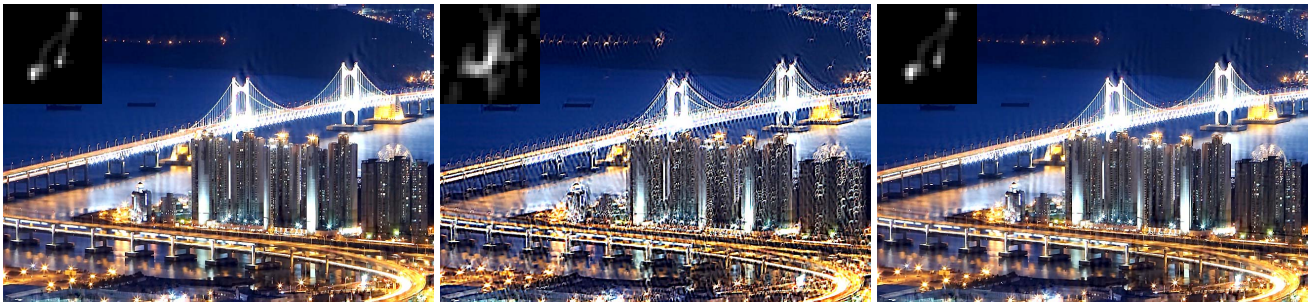

(j) Pan *et al*. [13] (k) Pan *et al*. [12] (l) Ours

Figure 17. Deblurred results on one synthetic image with numerous saturated areas and random noise. The proposed method generates clear images with fine details.

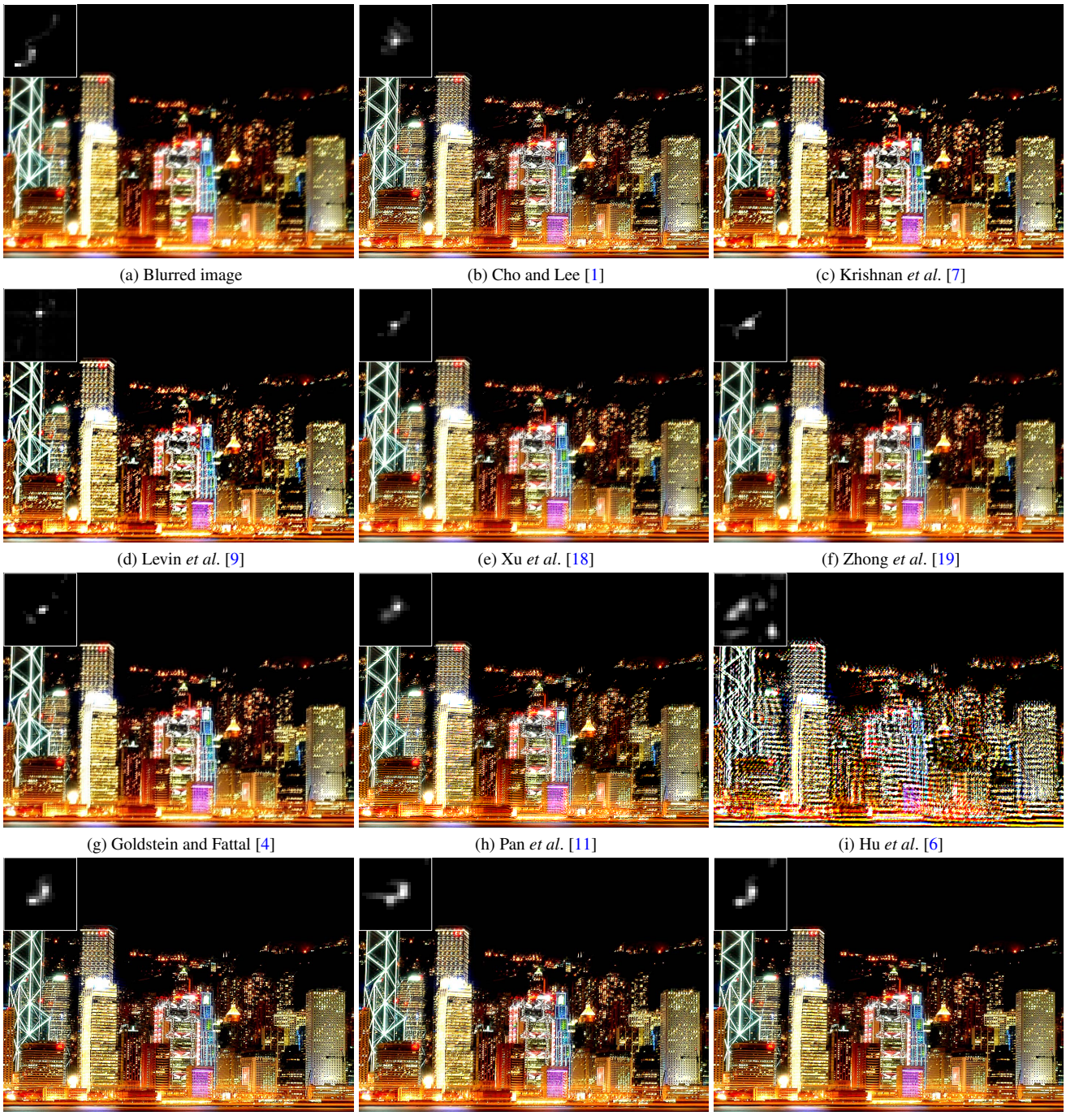

(a) Blurred image (b) Cho and Lee [1] (c) Krishnan *et al*. [7]

(d) Levin *et al*. [9] (e) Xu *et al*. [18] (f) Zhong *et al*. [19]

(g) Goldstein and Fattal [4] (h) Pan *et al*. [11] (i) Hu *et al*. [6]

(j) Pan *et al*. [13] (k) Pan *et al*. [12] (l) Ours

Figure 18. Deblurred results on one synthetic image with numerous saturated areas and random noise. The proposed method generates clear images with fine details.

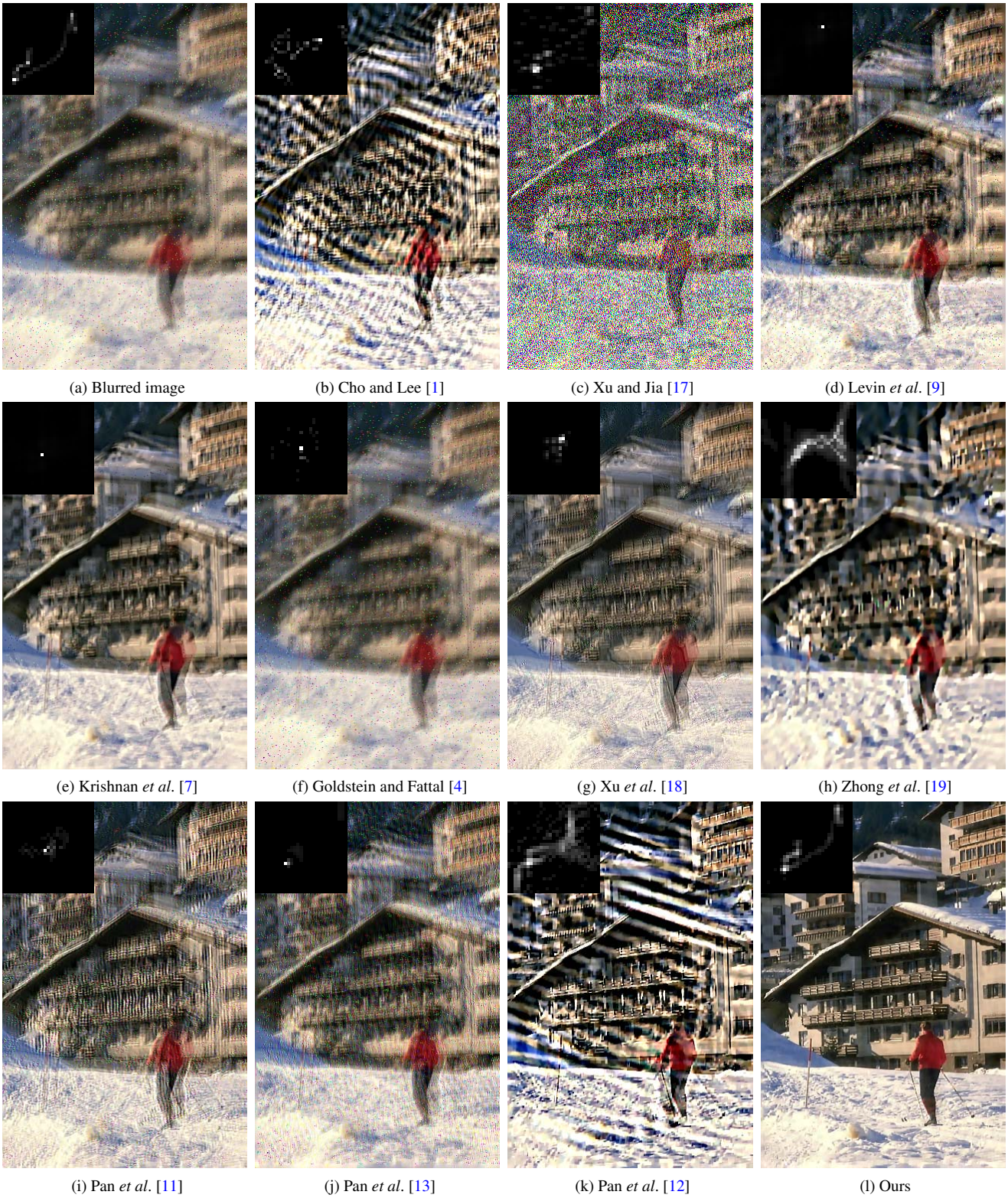

(a) Blurred image (b) Cho and Lee [1] (c) Xu and Jia [17] (d) Levin *et al*. [9]

(e) Krishnan *et al*. [7] (f) Goldstein and Fattal [4] (g) Xu *et al*. [18] (h) Zhong *et al*. [19]

(i) Pan *et al*. [11] (j) Pan *et al*. [13] (k) Pan *et al*. [12] (l) Ours

Figure 19. Deblurred results on one synthetic image with impulse noise. The proposed method generates clear images with fine details.

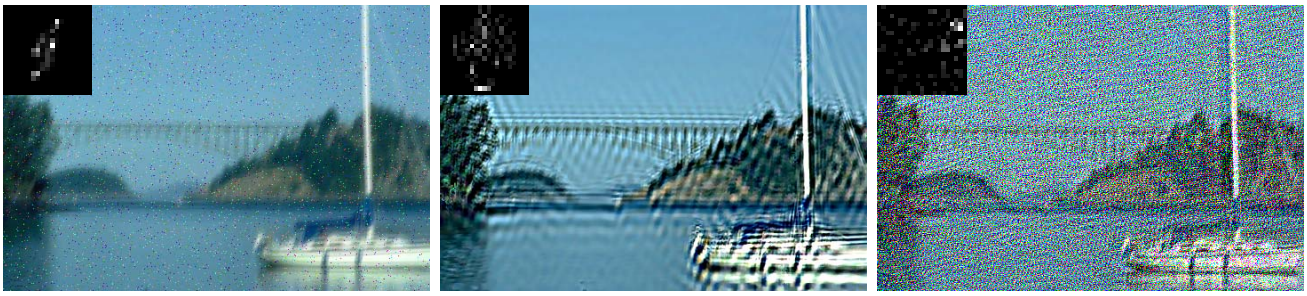

(a) Blurred image (b) Cho and Lee [1] (c) Xu and Jia [17]

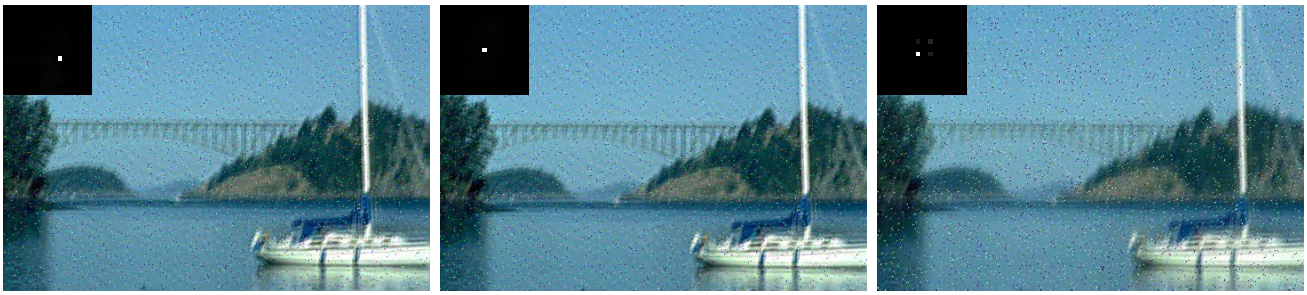

(d) Levin *et al*. [9] (e) Krishnan *et al*. [7] (f) Goldstein and Fattal [4]

(g) Xu *et al*. [18] (h) Zhong *et al*. [19] (i) Pan *et al*. [11]

(j) Pan *et al*. [13] (k) Pan *et al*. [12] (l) Ours

Figure 20. Deblurred results on one synthetic image with impulse noise. The proposed method generates clear images with fine details.

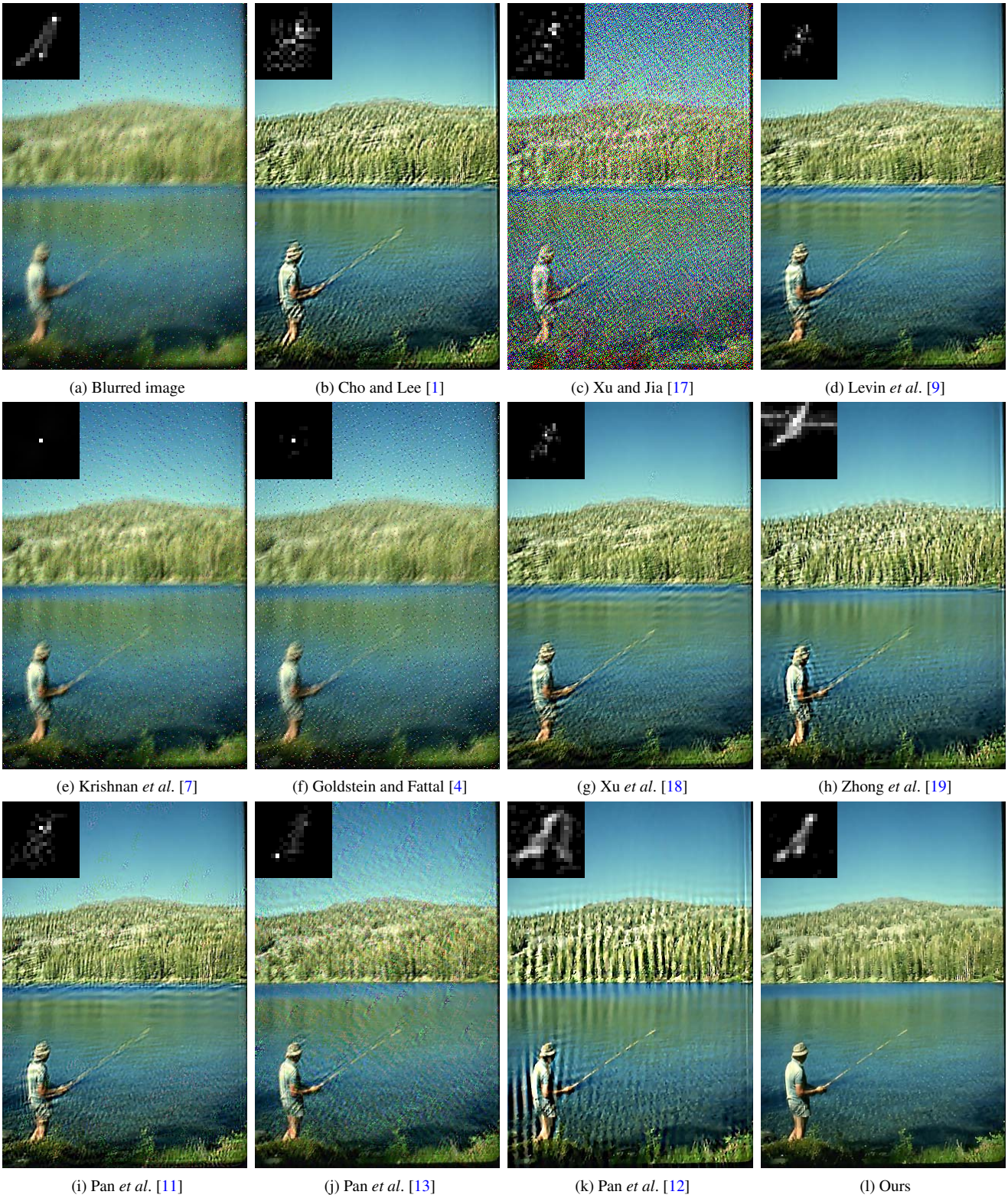

(a) Blurred image (b) Cho and Lee [1] (c) Xu and Jia [17] (d) Levin *et al*. [9]

(e) Krishnan *et al*. [7] (f) Goldstein and Fattal [4] (g) Xu *et al*. [18] (h) Zhong *et al*. [19]

(i) Pan *et al*. [11] (j) Pan *et al*. [13] (k) Pan *et al*. [12] (l) Ours

Figure 21. Deblurred results on one synthetic image with impulse noise. The proposed method generates clear images with fine details.

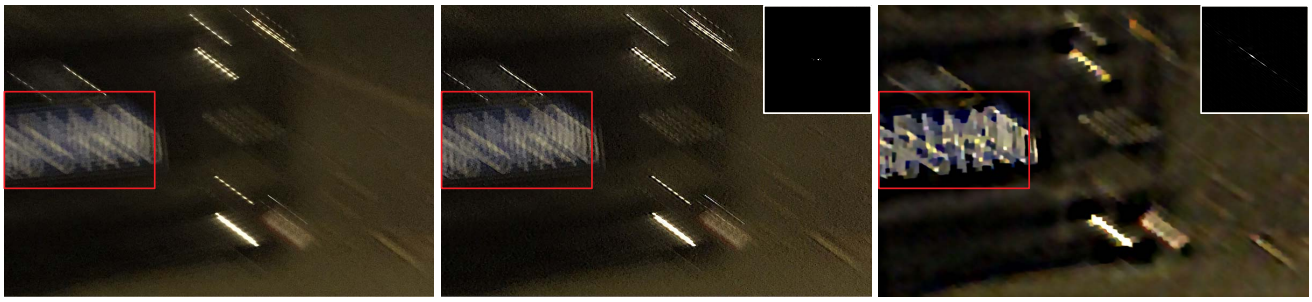

(a) Blurred image (b) Cho and Lee [1] (c) Krishnan *et al*. [7]

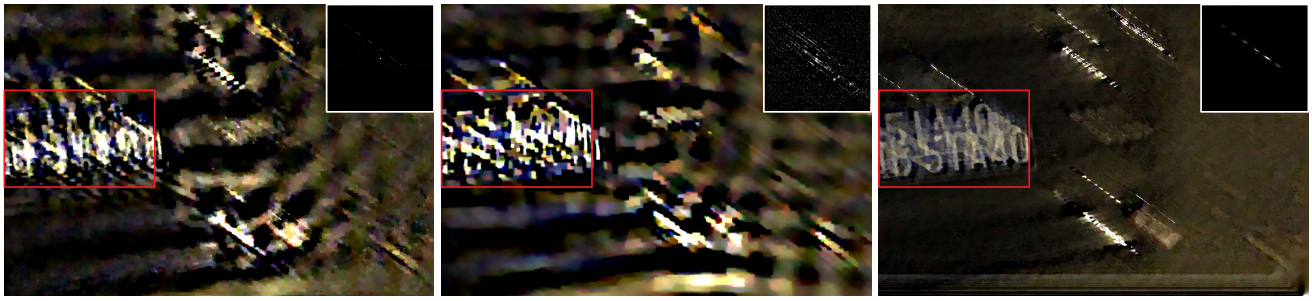

(d) Levin *et al*. [9] (e) Xu *et al*. [18] (f) Zhong *et al*. [19]

(g) Xu and Jia [17] (h) Pan *et al*. [11] (i) Hu *et al*. [6]

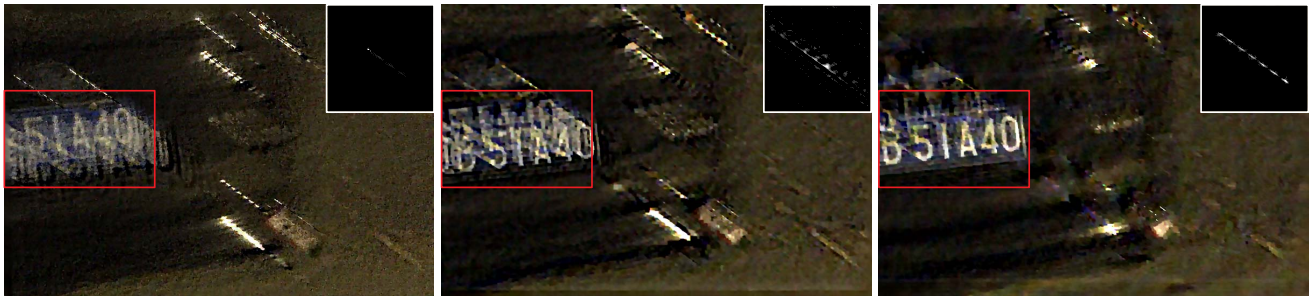

(j) Pan *et al*. [13] (k) Pan *et al*. [12] (l) Ours

Figure 22. Deblurred results on a real captured image with saturated areas and unknown noise. The proposed method generates the image with much clearer characters.

(a) Blurred image (b) Cho and Lee [1] (c) Krishnan *et al*. [7] (d) Levin *et al*. [9]

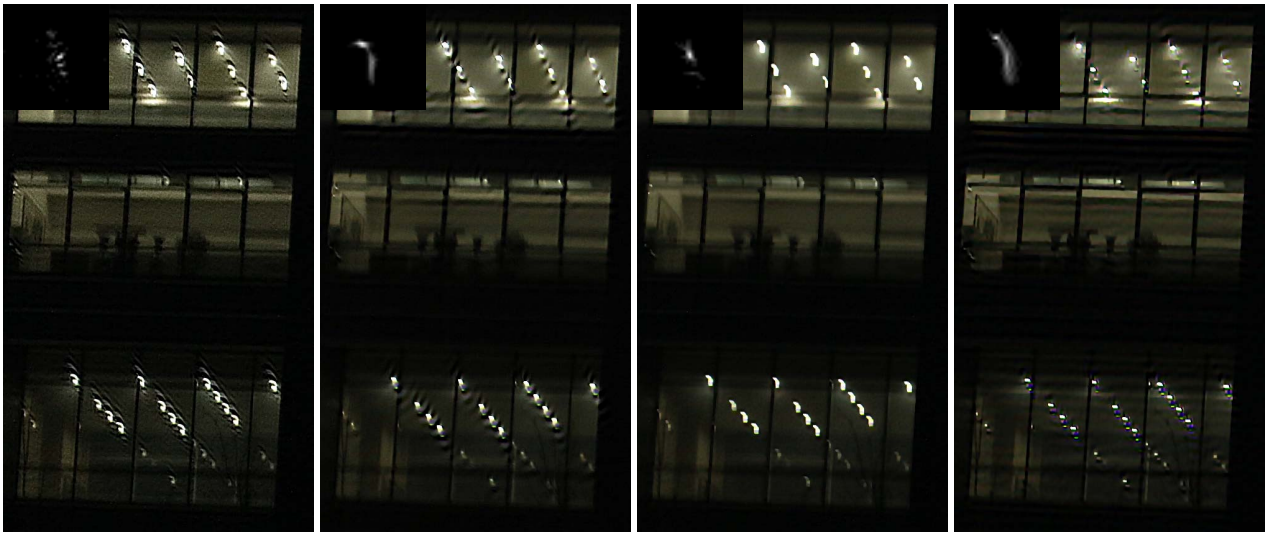

(e) Goldstein and Fattal [4] (f) Zhong *et al*. [19] (g) Xu *et al*. [18] (h) Pan *et al*. [11]

(i) Hu *et al*. [6] (j) Pan *et al*. [13] (k) Pan *et al*. [12] (l) Ours

Figure 23. A real captured image with saturated pixels and unknown noise. The proposed method generates clear images with much clearer structures.

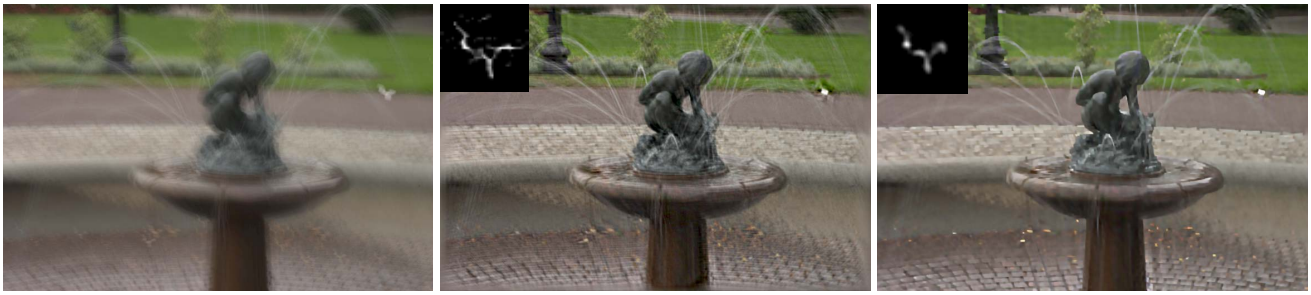

(a) Blurred image (b) Fergus *et al*. [3] (c) Ours

(a) Blurred image (b) Shan *et al*. [14] (c) Ours

(a) Blurred image (b) Cho and Lee [1] (c) Ours

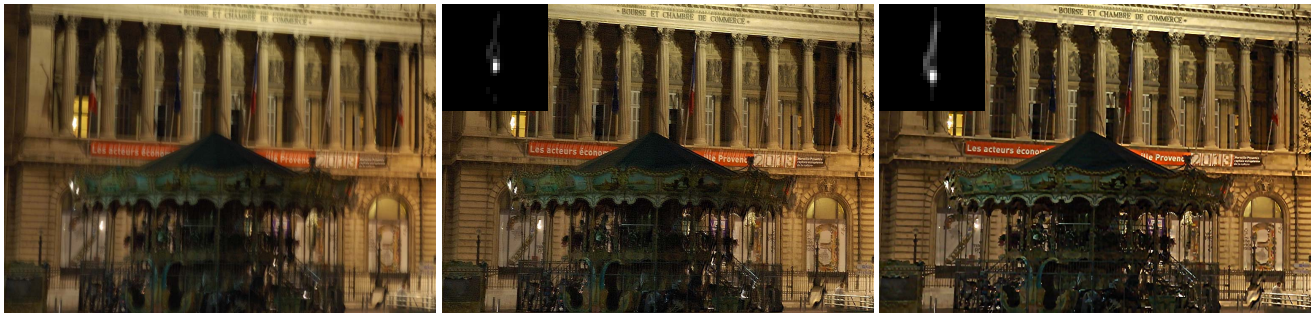

(a) Blurred image (b) Xu and Jia [17] (c) Ours

Figure 24. Comparison with state-of-the-art deblurring methods with their corresponding reported results. The proposed method generates comparable or even better results.

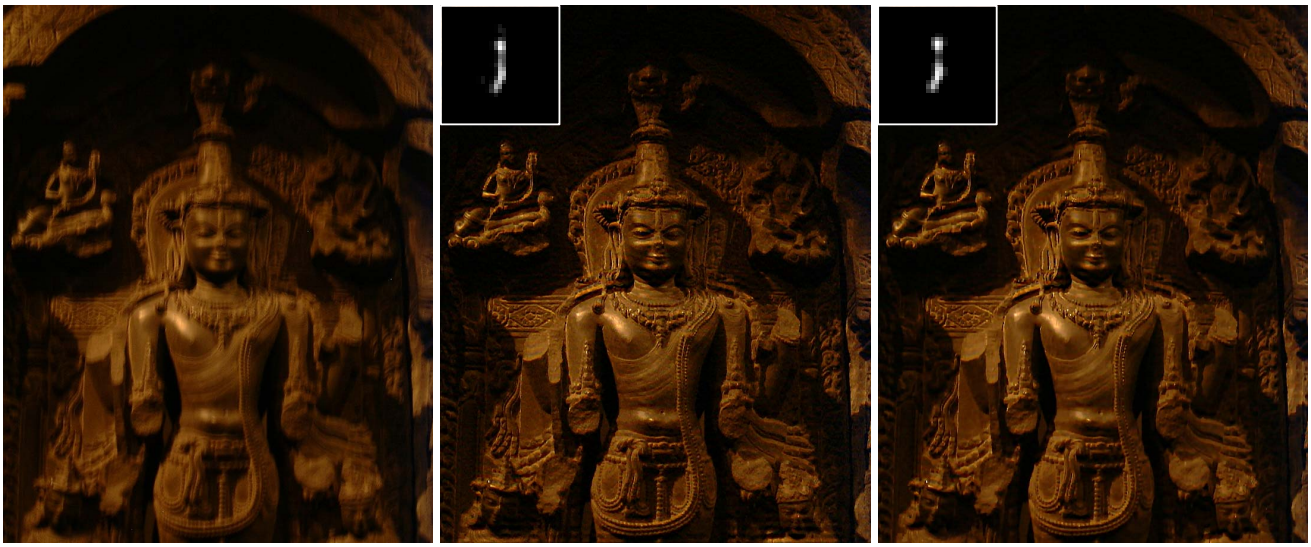

(a) Blurred image (b) Xu and Jia [17] (c) Ours

(a) Blurred image (b) Krishnan [7] (c) Ours

(a) Blurred image (b) Xu *et al*. [18] (c) Ours

Figure 25. Comparison with state-of-the-art deblurring methods. The proposed method generates much clearer images.

(a) Blurred image (b) Xu *et al*. [18] (c) Ours

(a) Blurred image (b) Zhong *et al*. [19] (c) Ours

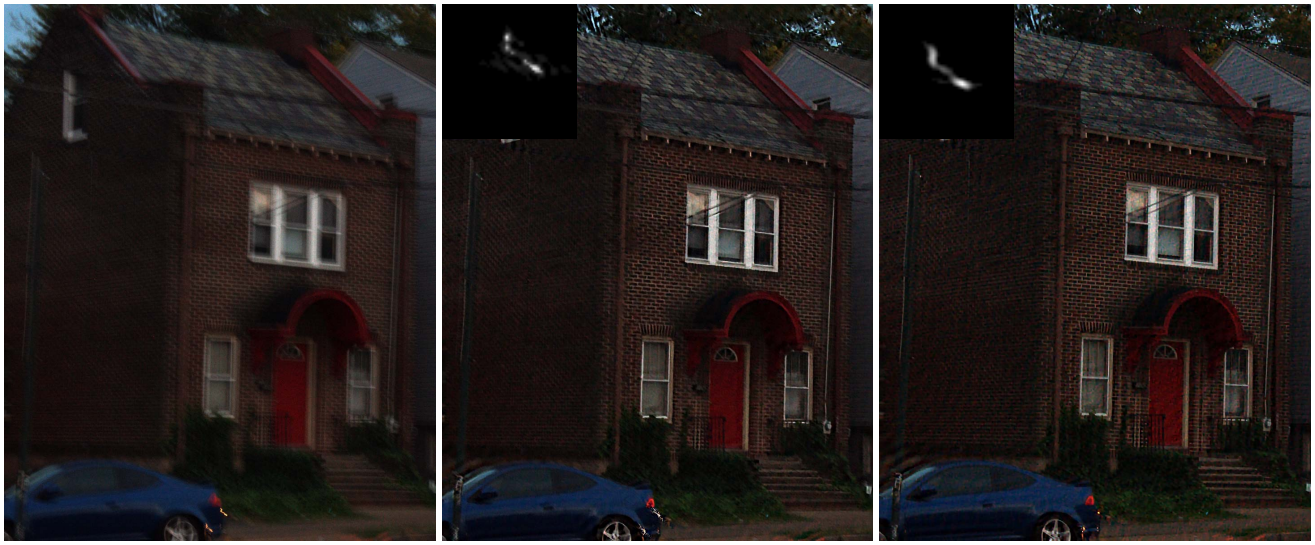

(a) Blurred image (b) Zhong *et al*. [19] (c) Ours

Figure 26. Comparison with state-of-the-art deblurring methods with their corresponding reported results. The proposed method generates much clearer images.

(a) Blurred image (b) Pan *et al*. [11] (c) Ours

(a) Blurred image (b) Pan *et al*. [13] (c) Ours

(a) Blurred image (b) Hu *et al*. [6] (c) Ours

Figure 27. Comparison with state-of-the-art deblurring methods with their corresponding reported results. The proposed method generates comparable or even better results.

(a) Blurred image (b) Hu *et al*. [6] (c) Ours

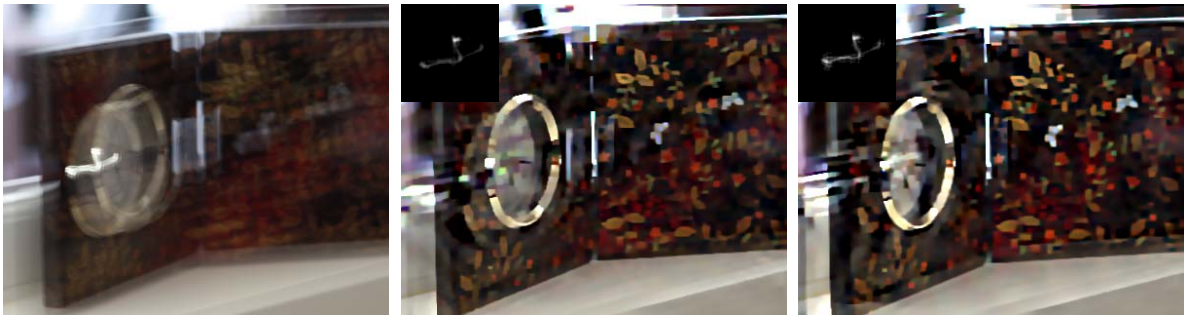

(a) Blurred image (b) Pan *et al*. [12] (c) Ours

(a) Blurred image (b) Pan *et al*. [12] (c) Ours

(a) Blurred image (b) Pan *et al*. [12] (c) Ours

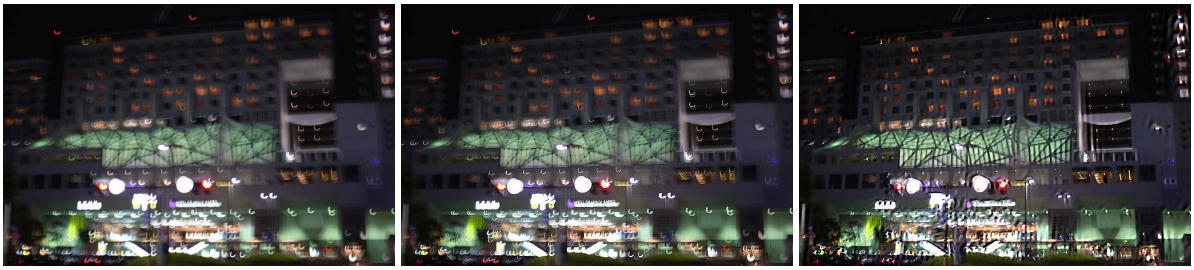

(a) Blurred image (b) Pan *et al*. [12] (c) Ours

Figure 28. Comparison with state-of-the-art deblurring methods for images with saturated areas. The proposed method generates much clearer images.

References

[1] S. Cho and S. Lee. Fast motion deblurring. *ACM TOG*, 28(5):145, 2009.

[2] S. Cho, J. Wang, and S. Lee. Handling outliers in non-blind image deconvolution. In *ICCV*, pages 495–502, 2011.

[3] R. Fergus, B. Singh, A. Hertzmann, S. T. Roweis, and W. T. Freeman. Removing camera shake from a single photograph. *ACM TOG*, 25(3):787–794, 2006.

[4] A. Goldstein and R. Fattal. Blur-kernel estimation from spectral irregularities. In *ECCV*, pages 622–635, 2012.

[5] M. Hirsch, C. J. Schuler, S. Harmeling, and B. Schölkopf. Fast removal of non-uniform camera shake. In *ICCV*, pages 463–470, 2011.

[6] Z. Hu, S. Cho, J. Wang, and M. H. Yang. Deblurring low-light images with light streaks. In *CVPR*, pages 3382–3389, 2014.

[7] D. Krishnan, T. Tay, and R. Fergus. Blind deconvolution using a normalized sparsity measure. In *CVPR*, pages 2657–2664, 2011.

[8] A. Levin, Y. Weiss, F. Durand, and W. T. Freeman. Understanding and evaluating blind deconvolution algorithms. In *CVPR*, pages 1964–1971, 2009.

[9] A. Levin, Y. Weiss, F. Durand, and W. T. Freeman. Efficient marginal likelihood optimization in blind deconvolution. In *CVPR*, pages 2657–2664, 2011.

[10] H. Liu, X. Sun, L. Fang, and F. Wu. Deblurring saturated night image with function-form kernel. *IEEE TIP*, 24(11):4637–4650, 2015.

[11] J. Pan, Z. Hu, Z. Su, and M. Yang. Deblurring text images via L_0-regularized intensity and gradient prior. In *CVPR*, pages 2901–2908, 2014.

[12] J. Pan, Z. Lin, Z. Su, and M.-H. Yang. Robust kernel estimation with outliers handling for image deblurring. In *CVPR*, pages 2800–2808, 2016.

[13] J. Pan, D. Sun, H. Pfister, and M.-H. Yang. Blind image deblurring using dark channel prior. In *CVPR*, pages 1628–1636, 2016.

[14] Q. Shan, J. Jia, and A. Agarwala. High-quality motion deblurring from a single image. *ACM TOG*, 27(3):73, 2008.

[15] L. Sun, S. Cho, J. Wang, and J. Hays. Edge-based blur kernel estimation using patch priors. In *ICCP*, 2013.

[16] O. Whyte, J. Sivic, and A. Zisserman. Deblurring shaken and partially saturated images. *IJCV*, 110(2):185–201, 2014.

[17] L. Xu and J. Jia. Two-phase kernel estimation for robust motion deblurring. In *ECCV*, pages 157–170, 2010.

[18] L. Xu, S. Zheng, and J. Jia. Unnatural L_0 sparse representation for natural image deblurring. In *CVPR*, pages 1107–1114, 2013.

[19] L. Zhong, S. Cho, D. Metaxas, S. Paris, and J. Wang. Handling noise in single image deblurring using directional filters. In *CVPR*, pages 612–619, 2013.